Metal-to-insulator transition in La1−xBaxTiO3

Veronika Fritsch, Joachim Hemberger, Manuel Brando, A. Engelmayer, Siegfried R. Horn, Matthias Klemm, Georg Knebel, Frank Lichtenberg, Prabhat Mandal, Franz Mayr, Michael Nicklas, Alois Loidl

Angaben zur Veröffentlichung / Publication details:

Fritsch, Veronika, Joachim Hemberger, Manuel Brando, A. Engelmayer, Siegfried R. Horn, Matthias Klemm, Georg Knebel, et al. 2001. "Metal-to-insulator transition in La1−xBaxTiO3." *Physical Review B* 64 (4): 045113. https://doi.org/10.1103/PhysRevB.64.045113.

Metal-to-insulator transition in $La_{1-x}Ba_xTiO_3$

V. Fritsch,[1] J. Hemberger,[1] M. Brando,[1] A. Engelmayer,[1] S. Horn,[2] M. Klemm,[2] G. Knebel,[1,3] F. Lichtenberg,[4] P. Mandal,[1,5] F. Mayr,[1] M. Nicklas,[1] and A. Loidl[1]

[1]*Experimentalphysik V, Elektronische Korrelationen und Magnetismus, Institut für Physik, Universität Augsburg, D-86135 Augsburg, Germany*

[2]*Experimentalphysik II, Institut für Physik, Universität Augsburg, D-86135 Augsburg, Germany*

[3]*CEA Grenoble, DRFMC/SPSMS/LCP, 38054 Grenoble Cedex 9, France*

[4]*Experimentalphysik VI, Elektronische Korrelationen und Magnetismus, Institut für Physik, Universität Augsburg, D-86135 Augsburg, Germany*

[5]*Saha Institute of Nuclear Physics, 1/AF, Bidhannagar, Calcutta 700 064, India*

(Received 19 October 2000; published 6 July 2001)

The ferroelectric insulator $BaTiO_3$ can be electron-doped by substitution of divalent Ba^{2+} with trivalent La^{3+}, creating d states at the transition-metal sites. The successive filling of the $3d$ Ti band initiates a sequence of electronic transitions. First, the system undergoes an Anderson-type insulator-to-metal-transition into a paramagnetic and metallic state, and second, a correlation-induced antiferromagnetic and insulating phase is established for La-rich concentrations. Ceramic $La_{1-x}Ba_xTiO_3$ samples covering the whole concentration range were systematically examined utilizing measurements of resistivity, specific heat, and magnetic susceptibility in the temperature range $1.8<T<300$ K. The concentration dependence of the Sommerfeld coefficient γ and the Pauli spin susceptibility was systematically investigated. The temperature dependence of the resistivity was studied in detail. In addition a (T,x) phase diagram of $La_{1-x}Ba_xTiO_3$ was constructed.

DOI: 10.1103/PhysRevB.64.045113 PACS number(s): 71.30.+h, 72.80.Ga

I. INTRODUCTION

Transition-metal oxides (TMO) belong to the most extensively studied class of materials in current solid state physics, revealing a huge variety of interesting and unconventional features, including high-temperature superconductivity, colossal magnetoresistance, and metal-to-insulator transitions (MIT).[1,2] The rich variety of systems, including the distinct possibilities of chemical substitution, provides the feasibility for systematic examinations of their physical properties by continuous variation of the intrinsic properties, such as structural parameters or valence. In this paper we systematically investigate the perovskite-type TMO $La_{1-x}Ba_xTiO_3$. $BaTiO_3$ is a ferroelectric insulator, crystallizing in the tetragonal structure at room temperature, the $3d$ band of Ti^{4+} being empty. Stoichiometric $LaTiO_3$ is a d^1 compound just on the insulating side of the Mott-Hubbard transition.[3] Doping $BaTiO_3$ with La^{3+} leads to a metallic phase due to a continuous filling of the conduction band. Further doping allows an investigation of the filling-controlled and correlation-induced Mott-Hubbard transition close to pure $LaTiO_3$. This transition has been extensively studied in the systems $LaTiO_{3+\delta}$ (Ref. 4) and $(La:Sr)TiO_3$ (Ref. 5). It is still unclear if the variation of the Ti-O-Ti bond angles, due to the different atomic radii of Sr^{2+} and Ba^{2+}, influences the $3d$-electron bandwidth.[1] The small splitting of the Hubbard bands in $LaTiO_3$ leads to a very sensitive dependence of the physical properties on the exact valence.[6–8] Accordingly, careful sample preparation and a systematic analysis of the exact stoichiometry are necessary because of their influence on the filling-dependent properties.

II. SAMPLE PREPARATION

Polycrystalline samples were prepared by argon arc-melting the stoichiometric mixture of $LaTiO_3$ and $BaTiO_3$, as described by Sunstrom and Kauzlarich.[9] This method was found to be advantageous to minimize impurity phases and grain boundaries and to produce compact ceramics. The latter is of importance with respect to the dc-transport measurements. The starting materials for the synthesis of $LaTiO_3$ were Ti_2O_3 (99.999% pure) and La_2O_3 (99.99% pure). $LaTiO_3$ was prepared by reacting La_2O_3 and Ti_2O_3. After grinding the components $BaTiO_3$ (99.9% pure) and $LaTiO_3$ were mixed in the stoichiometric ratios and pressed into pellets and afterwards melted in an arc furnace.

One $LaTiO_3$ sample, labeled (A), was prepared by zone melting in a mirror furnace. The oxygen content of this sample was determined by thermogravimetric analysis to be 2.99. As discussed later the antiferromagnetic transition temperature T_N was found to be 146 K, corresponding to the highest transition temperatures reported in literature.[4,10] Another $LaTiO_3$ sample, labeled (B), was prepared by argon arc-melting, as described in the previous paragraph.

In a correct composition the formula with the charge numbers would be

$$La_{1-x}{}^{3+}Ba_x{}^{2+}Ti_{1-x}{}^{3+}Ti_x{}^{4+}O_3{}^{2-}, \tag{1}$$

where every Ti^{3+} adds one d^1 electron to the conduction band. For a surplus or a deficiency of oxygen $\pm\delta$ and a deficiency of lanthanum $-y$ the electron concentration has to be calculated according to

$$La_{1-x-y}{}^{3+}Ba_x{}^{2+}Ti_{1-x-2\delta-3y}{}^{3+}Ti_{x+2\delta+3y}{}^{4+}O_{3+\delta}{}^{2-}, \tag{2}$$

for $y>0$. Due to the fact that the stoichiometry of Ti^{3+} determines the number of d^1 electrons, a deficiency of oxygen leads to a surplus of conduction electrons. In these cases it is unlikely that oxygen deficiency gives a Ti^{2+} oxidation

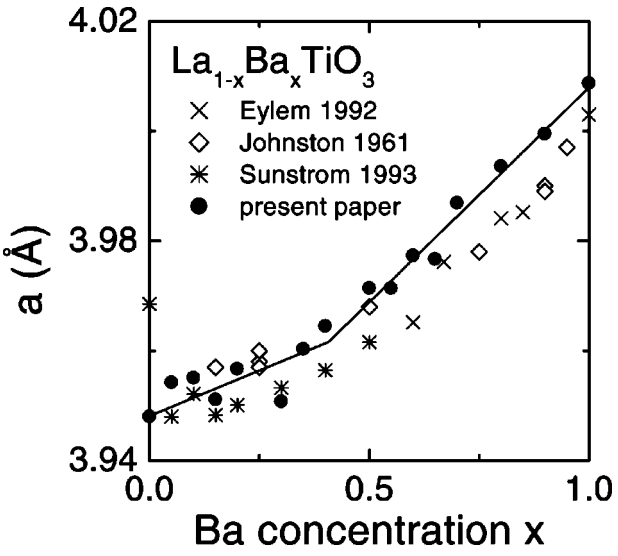

FIG. 1. Lattice parameter a of $La_{1-x}Ba_xTiO_3$ vs barium concentration x. The solid circles (●) are the values reported in the present paper; the other symbols represent values taken from literature (×, Ref. 12, ◇, Ref. 13, * Ref. 9). The solid line is drawn to guide the eye.

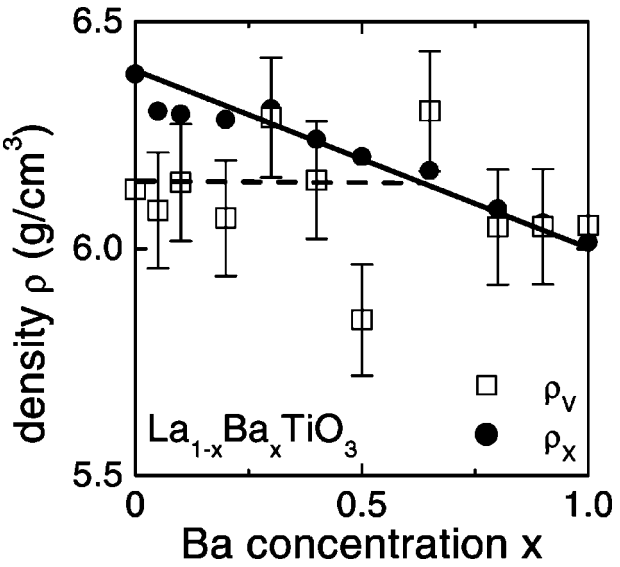

FIG. 2. Concentration dependence of the mass density ρ of $La_{1-x}Ba_xTiO_3$. The open squares indicate the densities ρ_V calculated from the macroscopic mass and volume of the samples; the solid circles indicate the densities ρ_X calculated from the lattice parameters of the unit cell and the nominal molar mass. For the latter values the error bars are comparable to the size of the symbols. The solid and dashed lines are drawn to guide the eyes.

state. Therefore one always expects positive values of δ. On the other hand, a surplus of oxygen as well as a deficiency of lanthanum leads to a deficiency of charge carriers in the $3d$ band.

III. SAMPLE CHARACTERIZATION

A. X-ray diffraction

All samples were characterized by x-ray diffraction. Taking into account the sensitivity of these investigations, we can exclude impurity phases with a volume fraction $>3\%$. The diffraction spectra were taken at room temperature. $BaTiO_3$ shows an almost cubic structure with a slight tetragonal distortion. Pure $LaTiO_3$ crystallizes in the orthorhombic $GdFeO_3$ structure.[11] $La_{1-x}Ba_xTiO_3$ samples investigated in this paper show a simple-cubic perovskite structure throughout the whole concentration range. It should be noted, that Eylem *et al.*[12] found an orthorhombic phase for $x<0.1$, a BaO-deficient cubic phase for $0.4<x<0.55$ and a cubic phase for $x>0.55$. The former two-phases were separated by an extended two-phase region. In Fig. 1 the lattice parameter a is plotted versus the barium concentration x as determined in the present paper together with data measured by Eylem *et al.*,[12] Johnston and Sestrich,[13] and Sunstrom and Kauzlarich.[9] The lattice parameters of the samples investigated in this paper are slightly larger in comparison to the literature values.[12,13,9] On the other hand Sunstrom and Kauzlarich[9] found a strongly enhanced lattice parameter for pure $LaTiO_3$, in disagreement according with the present results.

B. Density determination

The volume of the samples was determined by measuring the helium pressure change in two calibrated volumes with and without sample. This measurements were carried out using a pycnometer AccuPyc 1330 (Micromeretics GmbH). The density ρ_V can be calculated from the measured volume and mass. This value was compared to the density ρ_X resulting from the volume of the unit cell (determined from x-ray diffraction) and the nominal molar mass. ρ_V is directly influenced by lattice vacancies and off-stoichiometries, while ρ_X is dominated by intrinsic crystallographic effects. For a given concentration deviations of ρ_X and ρ_V allow us to draw conclusions about the existence of vacancies and about their deviations from the expected stoichiometry. The results of our measurements are shown in Fig. 2. The densities ρ_X as calculated from the lattice constants are continuously decreasing, while the Ba concentration x is increasing. This is to be expected as the ratio of the atomic masses of lanthanum and barium is smaller than the ratio of the ionic radii: the ratio of the atomic masses is 1.012, and the ratio of the ionic radii in an octahedral environment is 0.817. For $x=0$ the volumetrically determined density ρ_V is smaller and remains constant for $x\leqslant 0.5$. At higher Ba concentrations ρ_V slightly decreases and matches the values of ρ_X within the error bars. Already at the first sight this fact implies that off-stoichiometries become important only for Ba concentrations $0\leqslant x\leqslant 0.5$. Thus one expects a decreasing density with increasing barium concentration, as is found for ρ_X. The density ρ_V from the volume measurement is nearly constant over the whole concentration range. Most of the values of ρ_V appear to be lower than the values of ρ_X.

We suppose that the differences between ρ_X and ρ_V are caused by off-stoichiometries in the lanthanum and oxygen contents.[8,4] The effective molar mass of $La_{1-x-y}Ba_xTiO_{3-\delta}$ is given by

TABLE I. Deviations in composition of $La_{1-x-y}Ba_xTiO_3$ and $La_{1-x}Ba_xTiO_{3-\delta}$, calculated from density measurements [see Eq. (3)]. We assume that either δ or y is exactly stoichiometric. The values marked with an asterisk of $3-\delta$ make no physical sense. Here the off-stoichiometries are caused by the loss of lanthanum.

Sample	y	$3-\delta$
$LaTiO_3$ B	0.07	2.42*
$La_{0.95}Ba_{0.05}TiO_3$	0.06	2.49*
$La_{0.9}Ba_{0.1}TiO_3$	0.04	2.65*
$La_{0.8}Ba_{0.2}TiO_3$	0.05	2.49*
$La_{0.7}Ba_{0.3}TiO_3$	0.01	2.96*
$La_{0.6}Ba_{0.4}TiO_3$	0.01	2.79*
$La_{0.5}Ba_{0.5}TiO_3$	0.05	2.15*
$La_{0.35}Ba_{0.65}TiO_3$	−0.01	3.3
$La_{0.2}Ba_{0.8}TiO_3$	0.00	2.9
$La_{0.1}Ba_{0.9}TiO_3$	0.00	2.98
$BaTiO_3$	0.00	3.096

$$M_{\text{eff}}=(1-x-y)M_{\text{La}}+xM_{\text{Ba}}+M_{\text{Ti}}+(3-\delta)M_{\text{O}}=\frac{\rho_V}{\rho_X}M_n, \tag{3}$$

where M_n is the nominal molar mass ($y=0$, $\delta=0$). Assuming an ideal oxygen concentration ($\delta=0$) the value of lanthanum deficiency y can be calculated. δ can be determined in the same way considering a correct lanthanum stoichiometry ($y=0$). Equation (3) gives an estimate of the maximum oxygen deficiencies δ. The results are displayed in Table I.

There exists an unsettled dispute if the compounds close to $x=0$ rather reveal a lanthanum or an oxygen deficiency.[8] Most probably there will be a combination of deviations in both values y and δ, which cannot be resolved in this paper. The values in Table I give an estimate of the upper boundaries. However, as considered above, the oxygen vacancy should be smaller than the lanthanum deficiency, as Ti^{2+} ions are unlikely to be formed. As we will discuss later a deficiency of lanthanum and oxygen affects the physical properties of the system by changing the filling of the Ti $3d^1$ band. The number of conduction electrons decreases by a deficiency of La^{3+}, while it is enhanced by a deficiency of oxygen. However, it is immediately clear from Table I that the oxygen off-stoichiometries $3-\delta\approx 2.5$, marked with an asterisk, are much too large, because this would implicate the existence of Ti^{2+} ions. Despite the limited sensitivity of the above described method these unphysical results imply that stoichiometric deviations cannot be described as pure oxygen deficiency.

C. Scanning electron microscopy and energy dispersive x-ray analysis (EDX)

The surface of selected samples was examined with a scanning electron microscope. A typical image for $La_{0.1}Ba_{0.9}TiO_3$ is shown in Fig. 3. On a microscopic scale inhomogeneities concerning the degree of crystallization are observable. One can clearly distinguish different regions, regular shaped microcrystals with a typical size of 50 μm,

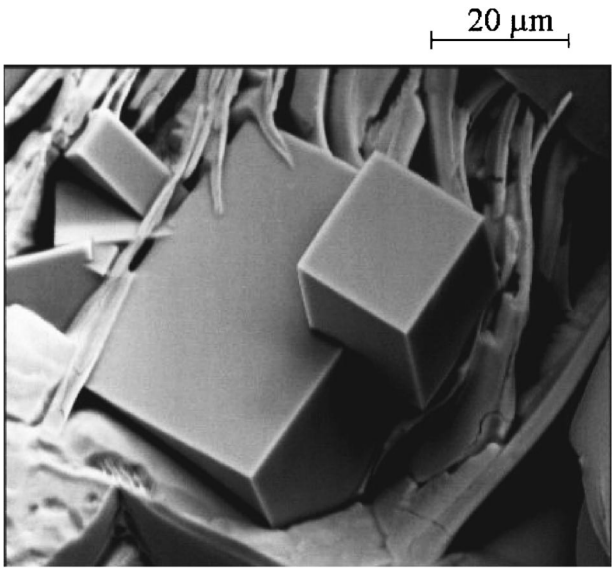

FIG. 3. Scanning-electron-microscope image of $La_{0.1}Ba_{0.9}TiO_3$ with a magnification of 1000.

embedded in less-crystallized threadlike structures. This type of inhomogeneity contrasts the situation in lanthanum-rich samples, such as $La_{0.8}Ba_{0.2}TiO_3$, where only one type of irregularly shaped grains is present.

At different surface positions EDX patterns were recorded for the compositions $La_{0.8}Ba_{0.2}TiO_3$ and $La_{0.1}Ba_{0.9}TiO_3$ in order to analyze the local stoichiometry. Due to the strong uncertainty in the evaluation of the oxygen emission line only the ratios Ba/Ti, La/Ti, and Ba/La were evaluated. The results are displayed in Table II together with the expected theoretical values. For $La_{0.8}Ba_{0.2}TiO_3$ no significant differences at different positions could be found, indicating a relatively high homogeneity of the sample. It has to be noted that the ratio Ba/Ti appears to be slightly higher than expected, while the ratio La/Ti is smaller than the theoretical value. This fact points towards a small lanthanum deficiency.[8] For $La_{0.1}Ba_{0.9}TiO_3$ the values of the local concentrations differ significantly. The regular shaped microcrystals revealed a higher barium and less lanthanum concentration than the threadlike regions (see Fig. 3).

IV. TRANSPORT, MAGNETIC PROPERTIES, AND SPECIFIC HEAT

The temperature dependence of the electrical resistivity has been measured in an Oxford ^{4}He cryostat by conven-

TABLE II. Ratio of elements in $La_{0.1}Ba_{0.9}TiO_3$ and $La_{0.8}Ba_{0.2}TiO_3$, determined from EDX analysis.

	Ba/Ti	La/Ti	Ba/La
$La_{0.1}Ba_{0.9}TiO_3$			
Microcrystalline cubic structures	0.78	0.17	4.63
Threadlike structures	0.84	0.07	11.55
Theoretical value	0.9	0.1	9
$La_{0.8}Ba_{0.2}TiO_3$	0.26	0.70	0.37
Theoretical value	0.2	0.8	0.25

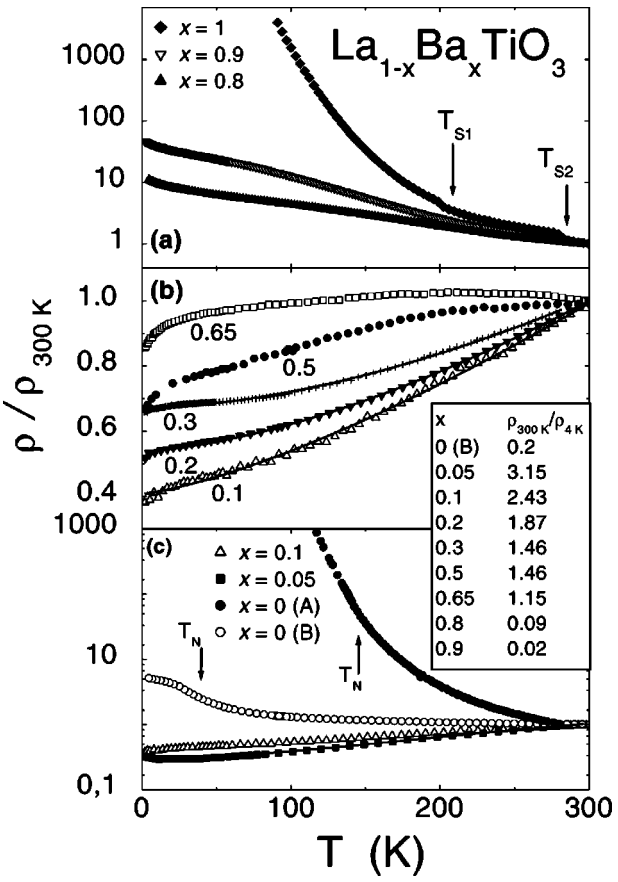

FIG. 4. Temperature dependence of the resistivity of $La_{1-x}Ba_xTiO_3$. The values are scaled with respect to $\rho(300\ \mathrm{K})$. The upper frame (a) shows $\rho(T)$ for concentrations $x=1$, $x=0.9$, and $x=0.8$. The middle frame (b) shows concentrations $0.65 \geqslant x \geqslant 0.1$. In the lower frame (c) the concentrations $x=0.1$ and $x=0.05$ are displayed. In addition, measurements of two samples of pure $LaTiO_3$ are shown. The crystal growth conditions of samples (A) and (B) are described in the text. The inset indicates the residual resistivities of the system investigated. The solid lines are fits with the parameters listed in Table III.

tional dc four-point techniques with currents between 0.1 and 1 mA for temperatures $1.8 < T < 300$ K. Magnetization experiments were carried out using a superconducting quantum-interference device (SQUID) magnetometer (Quantum Design) between 1.8 and 400 K in an external field up to 5 kOe. The temperature-dependent heat capacity was determined in an Oxford ^{4}He cryostat with a standard quasiadiabatic method for temperatures between 2.5 and 100 K.

A. Resistivity

The results of the resistivity measurements are shown in Fig. 4. The temperature dependence of the normalized resistivity has been plotted for a series of concentrations. For clarity the data are presented in three frames. The inset gives the residual resistivity values $\rho(300\ \mathrm{K})/\rho(4\ \mathrm{K})$ for most of the compounds. For the insulating samples with $x=0.9$ and $x=0.8$ the ratios are smaller than 1. With decreasing barium concentration x the residual resistivity values increase and drop again below 1 for the insulating $LaTiO_3$ sample (B). Figure 4(a) displays the resistivity of the barium-rich compositions with $x=1$, $x=0.9$, and $x=0.8$. The resistivity of pure (arc melted) $BaTiO_3$ was measured between 90 and 300 K. At $T=90$ K it is about four orders of magnitude larger than the resistivity of $La_{0.1}Ba_{0.9}TiO_3$. The structural transitions of $BaTiO_3$ from the tetragonal to the orthorhombic phase at 280 K and from the orthorhombic to the rhombohedral phase at 200 K are clearly observable. In the pure compound the conductivity is caused by thermally activated charge carriers and in the temperature range between 100 K and 200 K the resistivity can be described by an Arrhenius law with an energy gap of 170 meV. This value is much smaller than the energy gap of $BaTiO_3$ of 3.3 eV (Refs. 14 and 15). The difference can be explained by a well-defined impurity level close to the band edge. Probably this is due to a slight oxygen deficiency in this compound probably due to arc-melting.

TABLE III. Fit parameters obtained by using the fit function $\rho(T)/\rho_{300\ \mathrm{K}} = a + bT^c$ for the resistivity of samples with the concentrations $x=0.05$, 0.1, 0.2, and 0.3.

Sample	a	$b(10^{-5}\ \mathrm{K}^{-c})$	c
$La_{0.95}Ba_{0.05}TiO_3$	0.28	1.9	1.85
$La_{0.9}Ba_{0.1}TiO_3$	0.40	24.8	1.36
$La_{0.8}Ba_{0.2}TiO_3$	0.53	5.9	1.57
$La_{0.7}Ba_{0.3}TiO_3$	0.67	1.8	1.72

Doping the sample with small amounts of lanthanum leads to additional charge carriers in the $3d$ conduction band. The filling of the $3d$ band is the reason for the enhanced conductivity. The resistivity is still increased with decreasing temperature, but can no longer be described as purely thermally activated. Most probably, due to disorder effects, the charge carriers in the conduction band are localized below a mobility edge. Small anomalies are observable in the temperature derivatives of the resistivity in $La_{0.1}Ba_{0.9}TiO_3$ at 179 K and in $La_{0.2}Ba_{0.8}TiO_3$ at 82 K. No anomalies at these temperatures are detected in the magnetic susceptibility (see next section); thus a magnetic origin can be excluded. Similar phenomena were observed by Eylem *et al.*[12] in $La_{0.1}Ba_{0.9}TiO_3$ at 150 K. Johnston and Sestrich[13] already found that doping with lanthanum shifts the temperature of the transition from the cubic to the tetragonal phase below room temperature. Hence we can assign these anomalies in $\rho(T)$ to the structural phase transition.

Figure 4(b) shows the resistivity of the barium concentrations $x=0.65$, 0.5, 0.3, 0.2, and 0.1. The concentration-dependent insulator-metal transition takes place near $La_{0.35}Ba_{0.65}TiO_3$. At this doping level the slope of the resistivity curve $d\rho/dT$ changes sign at about 225 K. For lower barium concentrations the compounds behave as pure metal ($d\rho/dT > 0$). From the complex temperature dependence of ρ for $x=0.65$ and 0.5 we conclude that localization of charge carriers due to disorder still plays an important role in this concentration regime. Thus we find a filling-dependent metal-insulator transition, smeared out by Anderson-

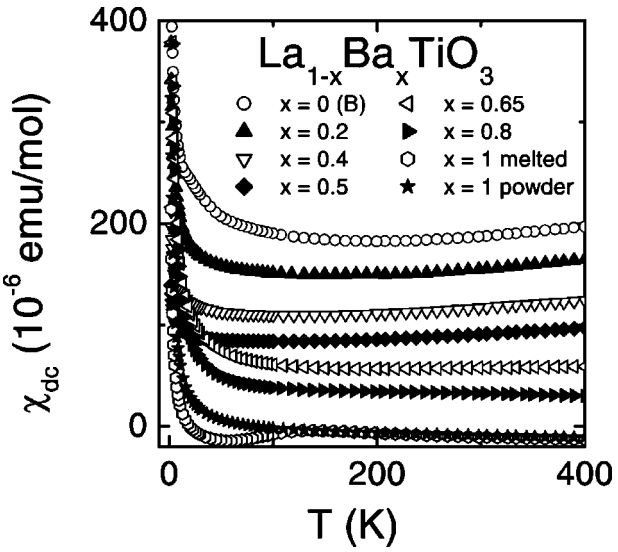

FIG. 5. Magnetic susceptibility χ of $La_{1-x}Ba_xTiO_3$, measured in an external magnetic field of 5 kOe. For pure $BaTiO_3$ results of highly stoichiometric powder and of argon-arc-melted samples are shown.

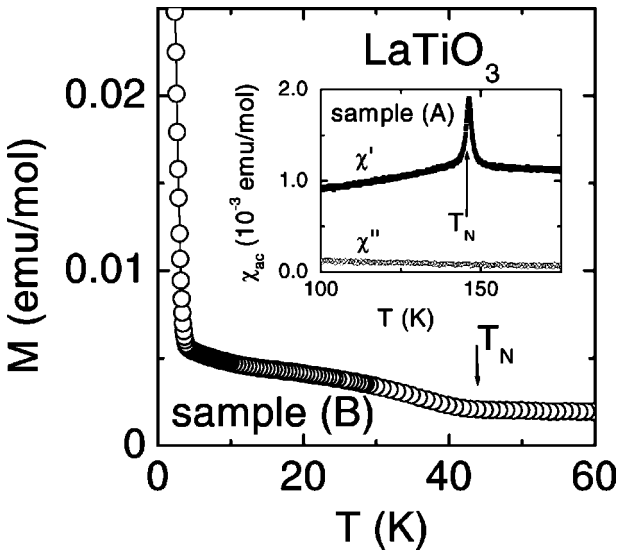

FIG. 6. Magnetization M vs temperature for $LaTiO_3$ sample (B) in an external field of 10 Oe. Inset: ac susceptibility of $LaTiO_3$ [sample (A)] in a stimulating magnetic field of 0.2 Oe_{rms} measured at a frequency of 3333 Hz.

localization effects. All resistivities reveal a downward curvature towards low temperatures. However, for barium concentrations $x<0.1$ the conductivities reveal a semiconducting characteristic at low temperatures, in agreement with the results of Sunstrom and Kauzlarich[9] and comparable to the measurements of Tokura *et al.* on $SrTiO_3$.[5] For concentrations $x=0.05$, 0.1, 0.2, and 0.3 the function $\rho(T)/\rho(300\ \mathrm{K})=a+bT^c$ was used to fit the data in a temperature range between 30 and 280 K. The results are given in Table III and as solid lines in Fig. 4(b). The fit parameter a, indicating the residual resistivity, increases with increasing barium concentration as expected. There are significant deviations from Fermi liquid behavior ($c=2$). Indeed, for low barium concentrations close to a phase transition at $T\rightarrow 0$ one expects exponents $1<c<2$. However, because of disorder and grain boundaries in ceramic samples this analysis should not be overestimated. But very interesting single crystal work is warranted.

A quantitative estimate of the absolute values of $\rho(T)$ is difficult. This fact results from the geometry of the samples and from the porous consistency with inner cracks and holes and a large volume fraction of grain boundaries. A rough estimation of the geometry provides a room temperature value of the resistivity about $\rho_{(300\ \mathrm{K})}\approx 100\ \mu\Omega\,\mathrm{cm}$ for the metallic samples, which corresponds to a conductivity $\sigma_{300\ \mathrm{K}}\approx 10^4\ \Omega^{-1}\,\mathrm{cm}^{-1}$. Raychaudhuri found in some metallic oxides near the metal-insulator transition a conductivity smaller than the Mott minimum of metallic conductivity. He calls these metallic states *marginal metallic*.[2] However, the conductivity of the metallic samples investigated in this paper is about an order of magnitude larger than the expected Mott minimum of conductivity, which usually is about $10^3\ \Omega^{-1}\,\mathrm{cm}^{-1}$ for d metals.[6] Probably the resistivity in the ceramic samples under investigation is still influenced by grain-boundary effects; therefore we expect even larger conductivities in single-crystalline samples.

In Fig. 4(c) the concentrations $x=0.1$ and $x=0.05$ are shown together with measurements on the two nominally pure $LaTiO_3$ samples (A) and (B). For $T<300$ K the sample with $x=0.1$ can be characterized as a poor metal, according to $d\rho/dT>0$ and the high value of ρ. For $La_{0.95}Ba_{0.05}TiO_3$, $d\rho/dT$ becomes negative for $T<20$ K and the resistivity shows a semiconducting characteristic. Obviously, electronic correlations have to be considered with increasing band filling and thus pure $LaTiO_3$ is a Mott insulator.[4,5,16] Both samples (A) and (B) show increasing resistivity with decreasing temperature. The oxygen content of sample (A), which was prepared by a floating zone method, was verified to be $LaTiO_{3\pm\delta}$ with $\delta\leqslant 0.01$. The discrepancies of the two $LaTiO_3$ samples (A) and (B), as shown in Fig. 4(c), can be explained by the sensitive dependence of the physical properties on the exact stoichiometry. The resistivity of $LaTiO_3$ [sample (A)] was fitted below the antiferromagnetic transition with an Arrhenius law $\rho(T)=\rho_0 e^{\Delta/2T}$, just like $BaTiO_3$. The energy gap was found to be $\Delta\approx 250$ meV. In literature the Mott-Hubbard gap, determined from optical spectroscopy,[11] is reported to be approximately 200 meV.

B. Magnetic susceptibility

The dc susceptibilities $\chi_{\mathrm{dc}}=M/B$ are shown in Fig. 5. $BaTiO_3$ is diamagnetic, all the other samples investigated were found to be paramagnetic. The susceptibility is almost temperature independent, as expected in the case of Pauli paramagnetism. For low temperatures all curves $\chi(T)$ show a strong Curie-like increase, probably caused by paramagnetic impurities, e.g., charge carriers localized at vacancies. Fitting these contribution with the Curie law and assuming spin $S=\frac{1}{2}$ impurities, one can estimate the number of defect states to be smaller than 0.3% for all samples. A systematic dependence of the defect concentration on x could not be observed.

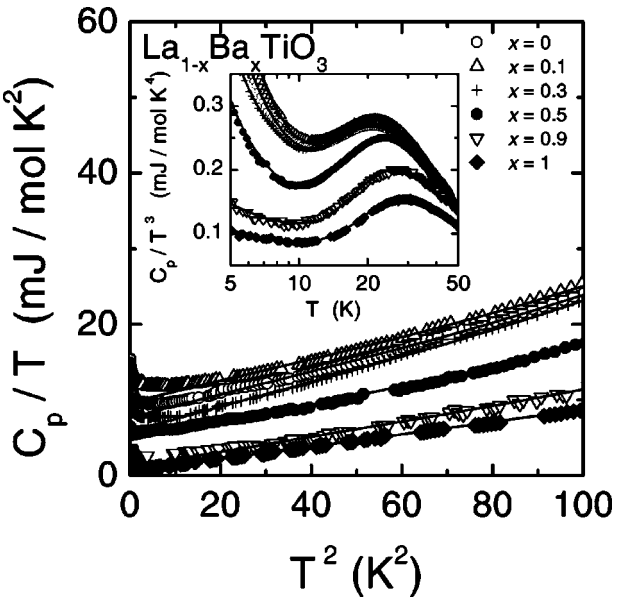

FIG. 7. Specific heat C_p of $La_{1-x}Ba_xTiO_3$ for concentrations $0 \leqslant x \leqslant 1$ vs temperature. The experimental results are plotted as C/T versus T. The solid lines are fits with the parameters listed in Table IV. The inset shows the specific heat values as C_p/T^3 versus T to display the strong deviations of the phonon density of states from the standard Debye model at low temperatures.

In addition to the temperature-independent contributions, i.e., diamagnetic core shells, Pauli-paramagnetic $3d$ electrons and the temperature-dependent Curie contribution of localized impurity spins, there is another temperature dependent contribution to the susceptibility, caused by localized states in the $3d$ band. That is why the $\chi(T)$ curves of the arc-melted samples show a broad minimum. This can easily be detected, e.g., for $x=0$ sample (B), close to 200 K. However, for $x=1$ the minimum is shifted to lower temperatures and additionally a maximum is observed. These anomalies can be explained by defect states at the upper edge of the band gap. They can be occupied by thermally activated electrons, the result being a paramagnetic contribution at high temperatures. For concentrations $x<0.9$ the maximum is shifted to temperatures above $T=400$ K due to the shift of the Fermi level with increasing band filling.

In Fig. 6 the magnetization M of $LaTiO_3$ sample (B) is displayed. For low temperatures there is a strong Curie-like increase of the magnetization, caused by paramagnetic impurities. The anomaly at 42 K indicates the transition into the antiferromagnetically ordered phase with the concomitant appearance of a small ferromagnetic moment. Comparing this value with the phase diagram of Lichtenberg *et al.*[4] an oxygen content of $\delta=0.09$ can be estimated. This is much smaller than the value calculated from the density determination, which was shown in Table I. On the other hand, according to a supposed deficiency of lanthanum,[8] we found a ratio La/Ti$\approx$0.90, which is in rough agreement to the values determined from the density measurements. This is another indication of the two competing deviations in stoichiometry of oxygen and lanthanum. The inset in Fig. 6 shows the ac susceptibility χ_{ac} of the sample $LaTiO_3$ sample (A).

TABLE IV. Results of the fit (for specific heat measurements of $La_{1-x}Ba_xTiO_3$) with the equation $C_{all,fit}=C_e(\gamma,T)+C_D(\theta_D,T)+C_E(\theta_E,r,T)$. Here γ is the Sommerfeld coefficient, θ_D the Debye temperature, θ_E the Einstein temperature, and r corresponds to the effective number of optical modes. Additionally the results of the magnetic susceptibility χ at $T=300$ K and the Wilson ratio $R_W=\chi/\gamma$ are shown.

x	γ (mJ/mol K^2)	θ_D (K)	θ_E (K)	r	$\chi_{300\,K}$ (μemu/mol)	R_W ($3\mu_B^2/\pi^2k_B^2$)
0	7.7	234	114	0.285	187	1.77
0.05	2.6	243	114	0.368	187	5.26
0.1	9.7	239	116	0.362	178	1.34
0.2	7.9	252	116	0.385	156	1.45
0.3	5.85	228	117	0.31	89.7	1.12
0.4	5.6	248	123	0.425	121	1.57
0.5	4.7	255	123	0.445	95.2	1.48
0.65	4.24	251	125	0.436	63.5	1.09
0.8	1.92	259	127	0.45	39.8	1.51
0.9	1.15	269	135	0.469	11.5	0.73
1	0.64	289	147	0.426	0	0

The peak at 146 K indicates the onset of antiferromagnetic order, close to the values reported in literature for stoichiometric samples.[4,10]

C. Specific heat

The results of the specific heat measurements on $La_{1-x}Ba_xTiO_3$ are illustrated in Fig. 7. For low temperatures $3<T<15$ K the electronic contributions to the specific heat $C_{el} \propto \gamma T$ dominate, which is demonstrated by a larger intercept in the linear dependence of C_p/T versus T^2. For temperatures below 3 K an increase of C_p/T is observed. The origin of this contribution is unclear. This increase is similar for magnetic (e.g., $x=0$) and nonmagnetic compounds (e.g., $x=1$) and therefore cannot be of magnetic origin. Lawless discussed a contribution of domain walls and grain boundaries, leading to an additional term $C \propto T^{3/2}$ at low temperatures,[17] which would be a possible explanation in our case. For the further evaluation of the data we restrict to temperatures $T>4$ K. To elucidate the significant deviations from the conventional phononic and electronic contribution the inset of Fig. 7 shows the temperature dependence of C_p/T^3 for temperatures below 50 K. In this representation a pronounced peak can be detected for all concentrations in the temperature region $20<T<30$ K. This additional contribution to the phononic specific heat can be explained by low-lying optical modes (Einstein modes), which yield significant deviations from the phononic density of states, thus leading to a pure T^3 dependence of the heat capacity at low temperatures ($T<\theta_D$). These kind of contributions are typical for all perovskites.[18] The position of the excess peak in C_p/T^3 is mainly determined by the Einstein temperature θ_E, because it is small in comparison to the effective Debye temperature θ_D of the lattice.[17] In this regime the specific heat can be described as a sum of Debye, Einstein, and electronic contributions: $C_p(T)=C_{el}(\gamma,T)+C_D(\theta_D,T)+C_E(\theta_E,r,T)$,

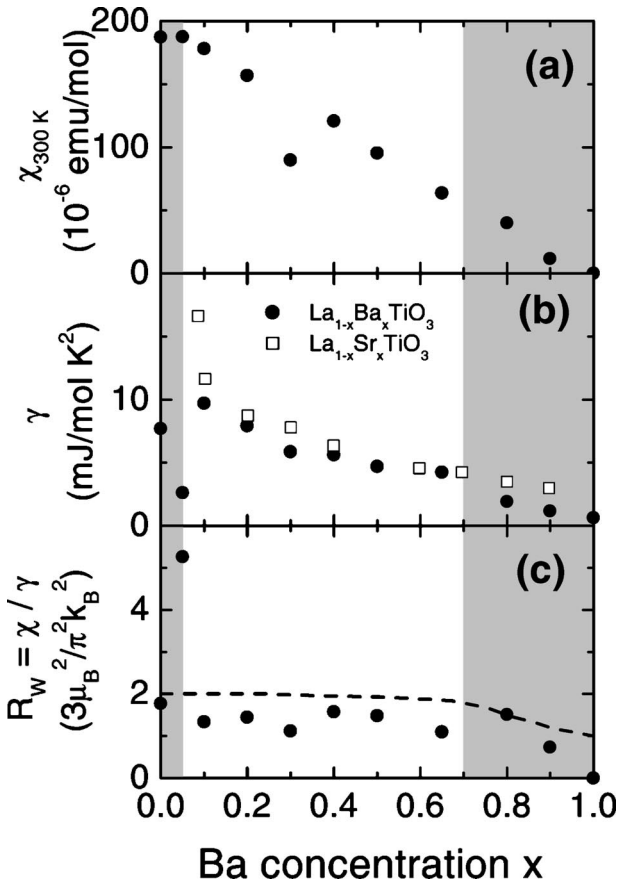

FIG. 8. (a) Magnetic susceptibility χ vs x at $T=300$ K, measured in a magnetic field of 5 kOe, (b) specific heat coefficient γ vs x [the values for La:$SrTiO_3$ are taken from Tokura *et al.* (Ref. 5)], and (c) Wilson ratio χ/γ as function of barium concentration in $La_{1-x}Ba_xTiO_3$. The dashed line is calculated as described in the text.

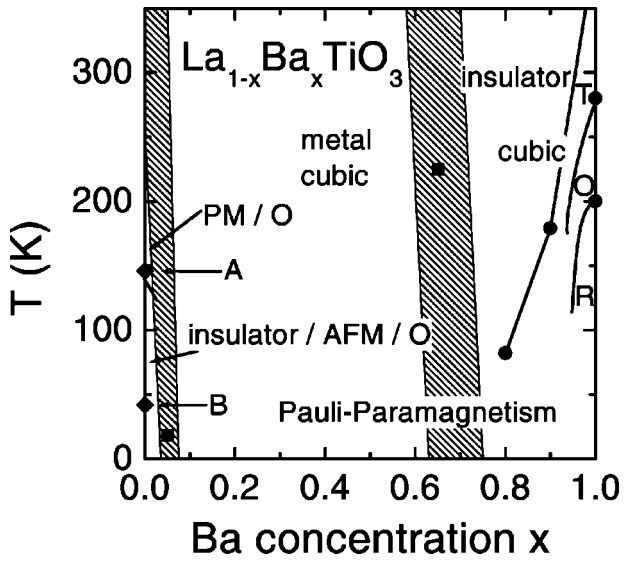

FIG. 9. Phase diagram of $La_{1-x}Ba_xTiO_3$. The crystal structures are labeled with T for tetragonal, O for orthorhombic, and R for rhombohedral. The magnetic structures are indicated as PM (paramagnetism) and AFM (antiferromagnetism). The hatched areas indicate crossover regimes from metallic (M) to insulating (I) behavior. The closed circles and the closed squares indicate structural phase transitions, the closed rhombs the onset of magnetic order.

where r is the effective number of the atoms contributing to the Einstein modes. The fit results are depicted as solid lines in Fig. 7. The corresponding fitting parameters are given in Table IV. The increase towards low temperatures, which rises with increasing doping, signals purely electronic contributions.

Pure $BaTiO_3$ reveals a Debye temperature $\theta_D=289$ K and differs slightly from the value found by Lawless ($\theta_D=252$ K).[17] The discrepancies of the values θ_D and θ_E found in literature can be explained by preparation effects. Henning and Hegenbarth[18] reported a great discrepancy between the Debye temperatures of two different samples $Ba_{0.4}Sr_{0.6}TiO_3$, depending on the preparation conditions. With decreasing Ba concentration x, both θ_D and θ_E decreases by about 20% in particular for $x\leqslant 0.3$. Henning and Hegenbarth[19] reported the dependence of the Einstein frequency on the mass of the A ion in $ATiO_3$ perovskites. However, this effect is not vigorous enough to explain the observed change in $\theta_E(x)$. A possible explanation could be the enhanced dielectric polarizability in the ferroelectric $BaTiO_3$.

The Sommerfeld coefficient γ and thus the specific heat at low temperatures $T\leqslant 10$ K increase with the band filling $(1-x)$ and the enhancement of the electronic correlations (see Table IV). For a parabolic band the relation $\gamma\propto m^* n^{1/3}$ is expected, where m^* is the effective mass and n the carrier density of the conduction electrons.[20] Tokura *et al.* verified the linear dependence of the band filling n on the La concentration $1-x$ in $La_{1-x}Sr_xTiO_3$ by Hall measurements.[5] For $x=0.5$ we found a value of $R_H=0.6$ cm^3/mC, comparable to the result presented for the Sr-doped system in literature.[5] The results for $\gamma(x)$ of $La_{1-x}Ba_xTiO_3$, provided by the fits with the parameters given in Table IV, are shown in Fig. 8(b). For a parabolic band the renormalized electronic density of states N is given by $N\propto(m^*)^{3/2}E_F^{1/2}$, with $E_F\propto(n_0)^{2/3}/m^*$, where n_0 is the carrier density and m^* the effective electron mass. Thus $\gamma\propto m^* n_0^{1/3}$, and one expects a dependence $\gamma\propto(1-x)^{1/3}$ for the Sommerfeld coefficient.[21] Clear deviations from this behavior can be recognized. The nonvanishing value for $x=1$ can possibly be explained by an overlap of Schottky-like domain-wall contributions at low temperatures. However, as discussed above, we should consider the existence of oxygen impurities which influence the band filling. For low barium concentrations γ is clearly elevated due to the electronic correlation-enhanced m^* in close analogy with the observations on $La_{1-x}Sr_xTiO_3$.[5] The values for γ found in this paper are slightly smaller than those reported for $La_{1-x}Sr_xTiO_3$.[5]

V. DISCUSSION AND CONCLUSIONS

A. Wilson ratio

Figure 8(a) shows the magnetic susceptibility χ at 300 K versus barium concentration x. The diamagnetic contribution of $BaTiO_3$, scaled with x, was subtracted. $\chi(300\text{ K})$ increases with decreasing content of barium. Pauli paramagnet-

ism is caused by moments of itinerant electrons near the Fermi level. Just as for the Sommerfeld coefficient γ one expects a $(1-x)^{1/3}$ dependence for the susceptibility $\chi(x)$. Again, the data presented in Fig. 8(a) do not resemble this behavior. So either the assumption of parabolic bands is much too oversimplified or the band filling does not depend linearly on the barium concentration.

The magnetic susceptibility χ and the Sommerfeld coefficient γ are expected to increase with increasing lanthanum concentration and reveal a divergence at the Mott-Hubbard transition.[1] However, the data presented in Figs. 8(a) and 8(b) do not reconcile this behavior. A closer inspection of Figs. 8(a) and 8(b) reveals that $\gamma(x)$ and $\chi(x)$ continuously increase with decreasing x towards the MIT close to $x=0.05$, but obviously far away from any critical behavior. Tokura *et al.*[5] found a similar behavior in $La_{1-x}Sr_xTiO_3$. For high strontium concentrations their data follow the calculated $(1-x)^{1/3}$ dependence and for low strontium concentrations a clear increase near the MIT is observed.

According to the picture of a Fermi liquid the susceptibility χ as well as the Sommerfeld coefficient γ depends linearly on the electronic density of states at the Fermi edge and thus on the effective mass m^*. As discussed above, the band filling should continuously increase with La doping, while m^* is expected to increase, due to electronic correlations, at the edge of the Mott-Hubbard MIT near half-filling of the Ti $3d$ conduction band. According to Brinkmann and Rice[22] the effective mass should diverge and in the vicinity of the Mott-Hubbard transition a critical behavior $m^* \propto 1/(\chi-\chi_c)$ is expected.[23] In spite of possible uncertainties, due to deviations from the exact stoichiometry, the significant enhancement of both quantities towards the critical concentration $x \approx 0.05$ can clearly be recognized.

Figure 8(c) displays the Wilson ratio $R_W=(\chi/\gamma)[3\mu_B^2/\pi^2 k_B^2]$. The Wilson ratio is close to 1 in Fermi liquids. Tokura *et al.* found $R_W=2$ in $La_{1-x}Sr_xTiO_3$, independent of the Sr concentration x (Ref. 5). Modeling the electron density of states by a parabolic band with the bandwidth of ~ 1 eV the Wilson ratio should rapidly increase from $R_W=1$ towards $R_W=2$ with increasing band filling and correlation strength. Model calculations are indicated as a dashed line in Fig. 8(c).[24] The experimentally observed values of R_W are slightly lower than expected for all concentrations, but they follow the model predictions in qualitative agreement, similar to the observations in $La_{1-x}Sr_xTiO_3$ (Ref. 5). The small increase of R_W towards higher La concentrations is due to magnetic correlations, which lead to an enhanced susceptibility, but do not increase the specific heat. The enhanced Wilson ratio for $x=0.05$ results from the low Sommerfeld coefficient due to the temperature-dependent MIT at 18 K for this concentration [see also the minimum in the resistivity displayed in Fig. 4(c)]. We would like to recall that the Wilson ratio was calculated with the susceptibility values at room temperature and thus reflects the correlated metallic state while the Sommerfeld coefficient was evaluated from the electronic specific heat in the low-temperature state, revealing a semiconducting behavior [see Fig. 4(c)]. Similar considerations have to be taken into account for pure $LaTiO_3$.

B. Phase diagram

From the experiments reported in this paper we were able to draw a (x,T) phase diagram (Fig. 9). $BaTiO_3$ is a diamagnetic and ferroelectric insulator. Below 400 K the structure changes from cubic to tetragonal. Two additional structural phase transitions are observable via anomalies in the temperature dependence of the resistivity: at $T=280$ K the transition into the orthorhombic and at $T=200$ K the transition into the rhombohedral structure. For concentrations $x=0.9$ and 0.8 remnants of the structural transition into the orthorhombic phase can be detected.

In addition, for pure $LaTiO_3$ a transition from an insulating paramagnetic phase at higher temperatures into the insulating antiferromagnetic ground state can be detected. At intermediate concentrations a broad metallic and paramagnetic regime is observed. Close to $x=0.7$ the MIT may be characterized as a disorder-induced transition into an insulating state, as the concentration of charge carriers is reduced. The MIT close to $x=0.05$ certainly is a correlation-induced phase transition into a Mott-Hubbard insulator.

C. Conclusion

We have investigated arc-melted ceramic samples in the whole concentration range for $La_{1-x}Ba_xTiO_3$ by x-ray diffraction, density measurements, and EDX analysis. Special attention was drawn to characterize the nature of possible stoichiometric deviations, such as lanthanum deficiency or oxygen surplus, which may sensitively influence the electronic properties of this system.The magnetic and transport properties were studied in detail. $BaTiO_3$ is a band insulator. By increasing the band filling $n=1-x$ of the Ti $3d$ band, a sequence of electronic transitions is induced. For $x>0.65$ the system remains insulating due to disorder-induced Anderson localization. At $x=0.05$ a second MIT appears, which is a correlation-derived transition into a Mott-Hubbard type insulator. The enhancement of γ and χ close to this transition is significant but remains finite ($\gamma \approx 10$ mJ/mol K^2). The Wilson ratio comes close to 2, indicative of a strongly correlated metal.

ACKNOWLEDGMENTS

We thank D. Vieweg, M. Müller, and A. Pimenova for sample preparation. This work was supported by the Bundesministerium für Bildung und Forschung (BMBF) under Contract No. EKM 13N6917/0 and by the Sonderforschungsbereich 484 (Augsburg) of the Deutsche Forschungsgemeinschaft.

[1] M. Imada, A. Fujimori, and Y. Tokura, Rev. Mod. Phys. **70**, 1039 (1998).
[2] A. K. Raychaudhuri, Adv. Phys. **44**, 21 (1995).
[3] I. Solovyev, N. Hamada, and K. Terakura, Phys. Rev. B **53**, 7158 (1996).
[4] F. Lichtenberg, D. Widmer, J. G. Bednorz, T. Williams, and A. Reller, Z. Phys. B: Condens. Matter **82**, 211 (1991).
[5] Y. Tokura, Y. Taguchi, Y. Okada, Y. Fujishima, T. Arima, K. Kumagai, and Y. Iye, Phys. Rev. Lett. **70**, 2126 (1993).
[6] N. F. Mott and E. A. Davies, *Electronic Processes in Non-Crystalline Materials* (Clarendon Press, Oxford, 1979).
[7] N. F. Mott, *Metal-Insulator Transitions* (Taylor and Francis, London, 1990).
[8] D. A. Crandles, T. Timusk, J. D. Garrett, and J. E. Greedan, Phys. Rev. B **49**, 16 207 (1994).
[9] J. E. Sunstrom and S. M. Kauzlarich, Chem. Mater. **5**, 1539 (1993).
[10] G. I. Meijer, W. Henggeler, J. Brown, O.-S. Becker, J. G. Bednorz, C. Rossel, and P. Wachter, Phys. Rev. B **59**, 11 832 (1999).
[11] Y. Okimoto, T. Katasufuji, T. Arima, and Y. Tokura, Phys. Rev. B **51**, 9581 (1995).
[12] C. Eylem, G. Sàghi-Szabo, B.-H. Chen, B. Eichhorn, J.-L. Peng, R. Greene, L. Salamanca-Riba, and S. Nahm, Chem. Mater. **4**, 1038 (1992).
[13] W. D. Johnston and D. Sestrich, J. Inorg. Nucl. Chem. **20**, 32 (1961).
[14] L. T. Hudson, R. L. Kurtz, S. W. Robey, D. Temple, and R. L. Stockbauer, Phys. Rev. B **47**, 1174 (1993).
[15] S. W. Robey, L. T. Hudson, C. Eylem, and B. Eichorn, Phys. Rev. B **48**, 562 (1993).
[16] Y. Taguchi, T. Okuda, M. Ohashi, C. Maurayama, N. Môri, Y. Iye, and Y. Tokura, Phys. Rev. B **59**, 7917 (1999).
[17] W. N. Lawless, Phys. Rev. B **14**, 134 (1976).
[18] I. Henning and E. Hegenbarth, Ferroelectrics **79**, 319 (1988).
[19] I. Henning and E. Hegenbarth, Phys. Status Solidi A **83**, K23 (1984).
[20] K. Kumagai, K. Kawano, T. Suzuki, H. Takahashi, M. Kasuya, Y. Fujishima, Y. Taguchi, Y. Okada, and Y. Tokura, Physica B **186-188**, 1030 (1993).
[21] K. Kumagai, T. Suzuki, Y. Taguchi, Y. Okada, Y. Fujishima, and Y. Tokura, Phys. Rev. B **48**, 7636 (1993).
[22] W. Brinkmann and T. Rice, Phys. Rev. B **2**, 4302 (1970).
[23] N. Kawakami and Y. Sung-Kil, Phys. Rev. Lett. **65**, 2309 (1990).
[24] J. R. Engelbrecht and K. Bedell, Phys. Rev. Lett. **74**, 4265 (1995).